



Cite this: DOI: 10.1039/c9cy01917k

# Self-tuned properties of CuZnO catalysts for hydroxymethylfurfural hydrodeoxygenation towards dimethylfuran production†

Magdalena Brzezińska,<sup>ab</sup> Nicolas Keller <sup>b</sup> and Agnieszka M. Ruppert <sup>\*a</sup>

5-Hydroxymethylfurfural (HMF) is a very valuable platform molecule obtained from biomass. It can be catalytically transformed to many industrially relevant products of both oxidation and reduction reactions. In this work, we showed that robust CuZnO can be an efficient, self-tuned catalyst for 2,5-dimethylfuran (DMF) (biofuel additive) synthesis. We showed that CuZnO catalysts can be further activated in the reaction environment and this process depends strongly on the initial catalyst properties and therefore on the catalyst preparation method. Smaller copper particles are more active but more prone to carbon deposit formation. Based on activity tests and extensive characterization, we have concluded that both Cu<sup>+</sup> and Cu<sup>0</sup> sites are necessary for high HMF conversion. While these two sites favor high conversion and high 2,5-bishydroxymethylfuran (BHMF) yield, the *in situ* formation of Lewis acid sites is proposed to be necessary for achieving a high DMF yield.

Received 22nd September 2019,  
Accepted 10th November 2019

DOI: 10.1039/c9cy01917k

rsc.li/catalysis

## Introduction

Fossil fuel depletion puts us in front of a challenge of finding an alternative source of both fuels and chemicals.<sup>1</sup> Among all the candidates, lignocellulosic biomass seems to be one of the most promising sustainable sources of raw carbon material, thanks to its abundance and the lack of competition with food production. Lignocellulosic biomass is therefore considered as a renewable source of platform molecules that have numerous potential applications in future biorefinery, chemical and material sectors.<sup>2</sup> In this frame, 5-hydroxymethylfurfural (HMF) is a very valuable platform molecule that can be obtained *via* a multi-step process initiated first by the acidic hydrolysis of lignocellulose. Thanks to its high functionalization, with both hydroxyl and carbonyl groups in the structure, HMF can be further catalytically transformed for *in fine* obtaining many industrially relevant products of both oxidation and reduction reactions.<sup>3,4</sup>

Scheme 1 illustrates the HMF hydrodeoxygenation reaction pathway, with the first step the HMF hydrogenation (pathway A) with the formation of 2,5-bishydroxymethylfuran

(BHMF) or its hydrodeoxygenation (pathway B) with the formation of 5-methylfurfural (5-MF). In the next step, BHMF undergoes a hydrodehydration reaction into 5-methylfurfuryl alcohol (5-MFA), while 5-MFA may also be obtained by hydrogenation of 5-MF. Next, 5-MFA undergoes hydrodehydration with the formation of 2,5-dimethylfuran (DMF) which can be further hydrogenated to 2,5-dimethyltetrahydrofuran (DMTHF). DMTHF may also be obtained *via* the hydrodeoxygenation of 2,5-bishydroxymethyltetrahydrofuran (BHMTHF), resulting from the hydrogenation of the C=C bonds in BHMF.

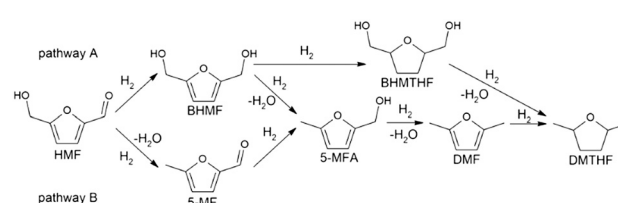
Among many valuable HMF-derived chemicals, 2,5-bishydroxymethylfuran (BHMF) and 2,5-dimethylfuran (DMF) gained a lot of interest. While BHMF can be potentially used as a substrate for biopolymer production, as it shows similar properties to crude oil-derived poly(ethylene terephthalate) and can successfully replace it,<sup>5,6</sup> DMF is thought to be used as a biofuel (notably as a cold-start fuel)<sup>7</sup> or as a biofuel additive without any change in the engine construction, thanks to physicochemical properties similar to those of gasoline and high octane number.<sup>8</sup>

<sup>a</sup> Institute of General and Ecological Chemistry, Faculty of Chemistry, Łódź University of Technology, ul. Żeromskiego 116, 90-924 Łódź, Poland.

E-mail: agnieszka.ruppert@p.lodz.pl; Fax: +48426313128; Tel: +48426313106

<sup>b</sup> Institut de Chimie et Procédés pour l'Energie, l'Environnement et la Santé, ICPEES, CNRS, University of Strasbourg, 25 rue Becquerel, 67087 Strasbourg, France

† Electronic supplementary information (ESI) available: Cell parameters of catalysts, Cu mean particle size during the cycling procedure, SEM image and STEM imaging of selected samples, XPS analysis. See DOI: 10.1039/c9cy01917k



Scheme 1 HMF hydrodeoxygenation reaction pathway.

Most of the studies are mainly devoted<sup>9–11</sup> to the synthesis of DMF through HMF hydrodeoxygenation, which was widely achieved with the use of catalysts based on noble metals such as Pd, Pt, Rh and Ru.<sup>9,10</sup> However, the restrictive use of additional acids such as H<sub>2</sub>SO<sub>4</sub>, HCl or acetic acid for promoting the dehydration step during the HMF conversion and the high price of noble metals are clearly the driving force behind the search for active, selective and stable noble metal-free catalysts for HMF conversion. So far, catalytic systems based on Ni, Co, Fe and Cu have been mainly investigated in the mentioned process<sup>9,10,12–14</sup> and it was shown that non-noble metals can be as active and selective as their noble metal counterparts while being more sustainable and allowing an easier selectivity control. Lilga *et al.* studied cobalt-based catalysts and evidenced that RANEY® Co and Co/SiO<sub>2</sub> allowed a similar performance to that of the Pt/Al<sub>2</sub>O<sub>3</sub> catalyst to be achieved under similar reaction conditions, with the absence of any DMF production and BHMF as the main product obtained.<sup>15</sup> Palkovits's group recently highlighted that higher HMF conversions were achieved on carbon-supported nickel catalysts using ether solvents such as THF or MTHF when compared to alcoholic solvents; however, the catalysts suffered from deactivation, while a very high hydrogen pressure of 100 bar and high nickel loadings were unfortunately necessary to reach a high DMF yield.<sup>16</sup> Although alumina-supported nickel catalyst could substitute for its palladium-based counterpart when water was used as a solvent, since both catalysts exhibited similar activity and selectivity profiles, Duarte *et al.* indicated that they both suffered from the absence of any DMF formation, while hydrogenation and dehydration products of HMF were observed like 5-MFA and furfuryl alcohol. The authors also evidenced that high selectivity to 5-MF and 5-MFA intermediates was observed on the copper-based counterpart catalyst, although the catalyst suffered from a moderate activity.<sup>17</sup>

As far as copper catalysts are concerned, copper chromite – an industrial hydrogenation catalyst – was one of the first catalysts studied in the HMF hydrodeoxygenation reaction thanks to the pioneering work by Dumesic's group who developed a process in which a sugar solution was directly converted into DMF with high selectivity (67%). Although the deactivation with time observed for the catalyst was overcome by performing regeneration under a hydrogen flow, both the high Cu loading and the high toxicity of chromium remained highly detrimental to the process and strategies for designing suitable catalysts still need to be implemented.<sup>18</sup> Due to the high affinity of Cu for the hydrogenation of carbonyl groups, copper-based catalysts are considered as promising systems for the HMF hydrodeoxygenation reaction.<sup>19</sup> In addition, the support itself needs to exhibit appropriate acidity in order to obtain DMF with high selectivity, and many studies highlighted the key role played by the support in the Cu catalyst behavior. Alumina was investigated as a Cu catalyst support due to its high acidity. However, although the Cu/Al<sub>2</sub>O<sub>3</sub> catalyst allowed DMF to be obtained as the main

reaction product after 140 min of test conducted at 175 °C under 20.7 bar of H<sub>2</sub>, the catalyst suffered from deactivation that resulted from the inhibition of the catalyst active sites through water molecule adsorption.<sup>20</sup>

Luque's group investigated Al-SBA15 aluminosilicate materials as Cu catalyst support and reported partial HMF dehydration into 5-methyl-2-furfuryl alcohol with 60% selectivity for short-time reactions due to the presence of acid centers and the use of microwave irradiation. Although higher selectivity was achieved through the incorporation of Zn into the structure of the support, this lowered the overall acidity of the system which inhibited proceeding side reactions, and only traces of DMF were observed in the reaction mixture.<sup>21</sup> Zhang *et al.* recently compared the behavior of highly loaded Cu catalysts (~20%) supported on different oxides (Al<sub>2</sub>O<sub>3</sub>, ZrO<sub>2</sub>, CeO<sub>2</sub>, ZnO). On the one hand, both Al<sub>2</sub>O<sub>3</sub> and ZnO supports allowed the highest DMF yields to be obtained as a result of the formation of the smallest Cu crystallite size among all tested supports.<sup>22</sup> On the other hand, high acidity and better utilization of the internal hydrogen generated from methanol in this study were reported as important factors in the case of Cu/Al<sub>2</sub>O<sub>3</sub> and Cu/ZnO catalysts, respectively. However, the reaction required operating at a relatively high temperature (240 °C) and for long reaction times (>6 h). Furthermore, the catalysts suffered from poor stability with the highest Cu leaching being obtained for the ZnO-supported catalyst.

The activity of different commercially available copper-based nanopowders (Cu, CuO, CuFe<sub>2</sub>O<sub>4</sub>, CuZnFe<sub>2</sub>O<sub>4</sub>, and CuZn) was investigated by Barta's group, among which the CuZn catalyst showed the highest activity and selectivity towards DMF when the reaction was performed in ethanol at 220 °C under 30 bar H<sub>2</sub> for 6 h.<sup>23</sup> This good catalytic performance was explained by the simultaneous presence of Zn<sup>2+</sup> cations which were identified as dehydration centers, and of Cu<sup>0</sup> acting as HMF hydrogenation centers. Further, the relatively small size of CuZn particles for a nanocomposite catalyst (<150 nm) was beneficial for obtaining a high DMF yield. Although the catalyst exhibited good stability with time in the reaction mixture, with no evidenced leaching despite the high Cu loading, the reaction selectivity was strongly reduced to achieve a level as low as 17% for the fourth cycle. In agreement with the dual nature of the CuZn catalyst surface developed in Barta's work, Zhu *et al.* optimized the Cu content of the catalyst at 54 wt% Cu for achieving full HMF conversion with high selectivity towards DMF when the reaction was performed at 220 °C under 15 bar of H<sub>2</sub> for longer than 5 h.<sup>19</sup> However, despite the use of a very high copper content, the CuZn catalysts turned out to be completely unstable during test cycles and were consequently suffering from a low HMF conversion of 30% at 10% selectivity to DMF after one single run.

The aim of this work is to investigate the key factors responsible for the high activity of CuZnO catalysts in the HMF hydrodeoxygenation reaction by studying the influence

of the preparation method of the catalysts on their catalytic properties.

A photoassisted method at room temperature was compared to a classical wet impregnation one with final temperature treatment. We showed that the choice of the preparation method and the chemical state of the Cu nanoparticles strongly influenced the catalyst activity and allowed the HMF hydrodeoxygenation selectivity to be tuned. Performing an oxidative treatment as an intrinsic part of the catalyst cycling protocol was reported to be crucial for both the performance and the stability of the catalysts.

## Experimental

### Support synthesis

ZnO was synthesized using a precipitation synthesis method in which 1.75 g of zinc(II) acetate dihydrate ( $\text{Zn}(\text{OAc})_2 \cdot 2\text{H}_2\text{O}$ , Sigma-Aldrich, Saint Louis, MO, USA, ACS reagent,  $\geq 98\%$ ) and 0.84 g of sodium carbonate ( $\text{Na}_2\text{CO}_3$ , Sigma-Aldrich, 99.5%) were dissolved under stirring in 50 mL of distilled water, respectively. Both aqueous solutions were mixed, and the obtained precipitate was aged at room temperature in the mother liquor for 24 h under continuous stirring. The suspension was further centrifuged for 30 min at 3500 rpm and finally washed and filtered under vacuum with distilled water. The resulting powder was dried at 100 °C for 12 h and subsequently calcined at a temperature of 300 °C for 2 h at a 10 °C  $\text{min}^{-1}$  heating rate.

### Catalyst preparation

**CuZnO catalyst prepared *via* the wet impregnation method.** The catalyst was prepared with a 10 wt% metal content using an aqueous solution of  $\text{Cu}(\text{NO}_3)_2$  (Chempur, pure) with a concentration of 5000  $\text{mg l}^{-1}$ . The ZnO support was impregnated with the salt solution and the catalyst suspension was aged for 24 h at room temperature before the excess solvent was evaporated at 100 °C. The sample was dried at 100 °C for 1 h before being calcined in flowing air at 300 °C for 2 h (heating rate of 10 °C  $\text{min}^{-1}$ ). After cooling to room temperature, the catalyst was reduced in a hydrogen flow (60  $\text{mL min}^{-1}$ ) for 1 h at a temperature within the 200–550 °C range at a heating rate of 10 °C  $\text{min}^{-1}$ . The non-reduced and reduced catalysts were labeled as CuZnO(I) and CuZnO(I)<sub>T<sub>red</sub></sub>, respectively, depending on the reduction temperature.

**Photon-assisted preparation of CuZnO catalysts.** The catalyst was prepared by irradiating with solar light an aqueous suspension of the ZnO support containing  $\text{Cu}(\text{NO}_3)_2$  as the copper precursor. The irradiation was provided using an Atlas Suntest XLS+ reaction chamber equipped with a xenon arc lamp adjusted to a 500  $\text{W m}^{-2}$  irradiance (with a 30  $\text{W m}^{-2}$  UV-A content) (320–800 nm wavelength range, ICH Q1B guidelines). The amount of copper precursor used was adjusted to have a Cu content of 10 wt% in the catalyst.

The dissolution of 38 mg of Cu(II) nitrate trihydrate (Sigma-Aldrich, p.a.) was performed in water at room

temperature before 90 mg of ZnO was dispersed under stirring in 100 ml of copper solution in a beaker-type glass reactor at a 0.38  $\text{g l}^{-1}$  concentration. Prior to irradiation, the suspension was stirred in the dark for 30 min at 60 °C to ensure the establishment of the adsorption/desorption equilibrium before the photon-assisted synthesis was performed under stirring under solar light for 2 h. The synthesis was monitored by UV-vis spectrophotometry by following the disappearance of the absorption peak at  $\lambda = 800$  nm. The catalyst was washed and filtered under vacuum several times with distilled water and finally dried at 100 °C for 1 h. The as-prepared sample was then labelled as CuZnO(P).

### Catalytic test

**5-Hydroxymethylfurfural hydrodeoxygenation.** In a typical 5-hydroxymethylfurfural hydrodeoxygenation experiment, 1 g of HMF, 0.3 g of a catalyst and 30 ml of dioxane were combined in a 60 ml Hastelloy autoclave. The reactor was pressurized with hydrogen to 30 bar and the temperature was maintained at 220 °C for 5 h. After the reaction time, the autoclave was cooled and the remaining pressure was released. The obtained reaction mixture was then centrifuged to separate the catalyst from the solution. The products were further analysed using an Agilent 7820A GC instrument equipped with a flame ionization detector and a CP-Wax 52 CB capillary column.

The activity of the catalysts was expressed in terms of HMF conversion and of reaction yield to given products, calculated as follows:

$$\text{Conversion} = \frac{n_{\text{HMF}_i} - n_{\text{HMF}_f}}{n_{\text{HMF}_i}} \times 100\%$$

$$\text{Yield}_p = \frac{n_p}{n_{\text{HMF}_i}} \times 100\%$$

where  $n(\text{HMF})_i$  and  $n(\text{HMF})_f$  are the number of moles of HMF molecules before and after the test, respectively, and  $n(\text{P})$  is the number of moles of a given product within the reaction mixture.

For assessing the catalyst recycling behavior, the catalyst was recovered from the reaction medium by centrifugation, with a subsequent washing with deionized water and a final drying step.

### Catalyst characterization

X-ray diffraction (XRD) measurements were collected using a D8 Advance Bruker diffractometer operating in  $\theta/\theta$  mode. The X-ray source was a Cu long fine focus X-ray diffraction tube operating at 40 kV and 40 mA, with  $\text{K}_{\alpha 1}$  radiation at  $\lambda = 1.5406$  Å. Data were collected in the 20–85°  $2\theta$  range with a 0.0263° scan step and a 0.6 s step time. Some patterns have been investigated by Rietveld refinement using Fullprof

software for which the modified Thompson–Cox–Hastings function was chosen to generate the line shape of the diffraction peaks. Instrumental broadening has been previously determined by measuring the scattering from corundum (NIST standard SRM 1976b).<sup>24,25</sup>

Temperature-programmed reduction (TPR) was performed on an AMI1 system from Altamira Instruments, USA, equipped with a thermal conductivity detector and was used for examining the reducibility of catalysts. All the catalysts prepared through the wet impregnation method were calcined at 300 °C (at a 10 °C min<sup>-1</sup> heating rate) for 30 min in a mixture of 2 vol% O<sub>2</sub> and 98 vol% Ar at a space velocity  $W/F = 1.11 \times 10^{-5} \text{ g h}^{-1} \text{ cm}^{-3}$  before the TPR profiles were recorded from 35 °C up to 800 °C, at a heating rate of 7 °C min<sup>-1</sup>, using a mixture of 5 vol% H<sub>2</sub> and 95 vol% Ar at a similar space velocity.

Scanning electron microscopy (SEM) was performed in secondary electron mode on a JEOL JSM-6700 F FEG microscope.

Transmission electron microscopy (TEM) was performed using a JEOL 2100F instrument with a point resolution of 0.2 nm. A Mo grid was used for performing EDS analysis of Cu–ZnO samples. The interplanar spacings were calculated using ImageJ software.

Secondary ion mass spectra were recorded using a time-of-flight secondary ion mass spectrometer (ToF-SIMS IV) manufactured by ION-TOF GmbH, Germany, equipped with a 25 kV pulsed Bi<sup>3+</sup> primary ion gun working in the static mode. The measurements were performed in the static mode. The samples were pressed into pellets and then fixed to the sample holder by double-sided tape. The analyzed area of the sample surface was 500 μm × 500 μm. During analysis, a pulsed low-energy electron flood gun was used for charge neutralization. The experiments were repeated three times for each sample.

Acetone-adsorbed FTIR measurements were carried out using a Nicolet 6700 FTIR spectrometer equipped with an

MCT detector made by Thermo Scientific, using a drift cell. Before measurement, the samples were treated following the same procedure used to prepare the catalysts. After cooling to 40 °C in an Ar flow, acetone sorption was first performed for 20 min and the chamber was further purged with an Ar flow for 20 min to get rid of gaseous acetone. All spectra were recorded with a time interval of 2 min in a wavenumber range of 1800–1600 cm<sup>-1</sup>, with a scan number of 64 and a spectral resolution set at 4 cm<sup>-1</sup>, and using a 20 ml min<sup>-1</sup> gas flow.

X-ray photoelectron spectroscopy (XPS) characterization was performed on a ThermoVGMultilabESCA3000 spectrometer (Al Kα anode at  $h\nu = 1486.6 \text{ eV}$ ). The energy shift due to electrostatic charging was subtracted using the adventitious sp<sup>2</sup> carbon C1s band at 284.6 eV. Contributions with a Doniach–Sunjic shape<sup>26</sup> and an ‘S-shaped’ Shirley-type background<sup>27</sup> were used.

Measurements of Cu and Zn content in the postreaction mixture were performed with flame atomic absorption spectrometry (FAAS) using a Unicam Solaar M6 atomic absorption spectrometer.


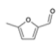



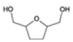
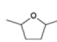
## Results

### Catalytic activity

**Influence of pretreatment.** Table 1 shows the influence of the reduction pretreatment conditions on the performance of the CuZnO catalysts prepared *via* the impregnation method. The CuZnO(I) catalyst pre-reduced at the high temperature of 550 °C exhibited a marginal HMF conversion.

Interestingly, by lowering the reduction temperature from 550 °C to 200 °C, the HMF conversion gradually increases up to 41%, accompanied by a slight increase in the BHMF selectivity. The non-reduced CuZnO(I) catalyst allowed reaching almost full HMF conversion (99%), together with a high selectivity to BHMF. As a result, the highest yield to BHMF of 93% was obtained on the oxidized CuZnO(I) catalyst.

**Table 1** Influence of the reduction pretreatment conditions on the activity of CuZnO catalysts in HMF hydrodeoxygenation

Catalyst	HMF conv. [%] 	Product yield [%]					
		5-MF 	BHMF 	5-MFA 	DMF 	BHMTHF 	DMTHF 
CuZnO(I)550 <sup>a</sup>	4	1	2	0	0	0	0
CuZnO(I)400 <sup>a</sup>	12	2	6	0	0	0	0
CuZnO(I)300	16	1	7	0	0	0	0
CuZnO(I)200	41	2	36	1	0	0	0
CuZnO(I)	99	2	93	2	0	0	0
Cu/Al <sub>2</sub> O <sub>3</sub> <sup>b</sup>	21	15	0	1	5	0	0

Reaction conditions: 220 °C; 5 h; 0.3 g of catalyst; 1 g of HMF; 30 ml of dioxane; 30 bar hydrogen. <sup>a</sup> Some by-products in small amounts were detected but not identified. In addition to the accuracy of the measurements at low conversion, this can explain the slight mismatch in the closure of the carbon balance. <sup>b</sup> A reference Cu/Al<sub>2</sub>O<sub>3</sub> benchmark catalyst was prepared *via* wet impregnation with a 10 wt% metal content using an aqueous solution of Cu(NO<sub>3</sub>)<sub>2</sub>. The γ-Al<sub>2</sub>O<sub>3</sub> (Fluka) support was impregnated with the metallic salt solution and the catalyst suspension was aged for 24 h at room temperature before the excess solvent was evaporated using a rotary evaporator. The sample was dried at 100 °C for 1 h before being calcined in flowing air at 300 °C for 2 h. After cooling to room temperature, the catalyst was further reduced in a hydrogen flow for 1 h at 300 °C.



These observations are in contrast to the literature concerning Cu catalysts supported on various oxides such as Al<sub>2</sub>O<sub>3</sub>, CeO<sub>2</sub>, TiO<sub>2</sub> or ZnO used for HMF conversion, for which a pre-reduction step at high temperature is usually required.<sup>19,20,22,28,29</sup>

Interestingly, the CuZnO catalyst without any pre-reduction treatment was more active than the Cu/Al<sub>2</sub>O<sub>3</sub> catalyst, which is actually considered as the reference benchmark catalyst,<sup>22</sup> and that showed a conversion as low as 21% with only 15% yield to 5-MF under our reaction conditions.

**Influence of reaction time.** The activity profile was influenced by the reaction time for the CuZnO(P) catalyst (Table 2). Although a high HMF conversion of 93% was reached already for 1 h of reaction, the DMF yield remained only moderate at 48%. Extending the reaction time allowed reaching a much higher DMF yield of nearly 80%, giving traces of intermediate reaction products like BHMF and 5-MFA and a very low yield of further C=C hydrogenation product DMTHF (9%).

The situation was fully different in the case of the CuZnO(I) catalyst. Already almost full conversion was reached after only 0.5 h of reaction giving a full selectivity to BHMF. BHMF is obtained *via* C=O bond hydrogenation from HMF and although it is an intermediate product in the DMF production, the reaction selectivity to BHMF however remained constant for the 5 h of the reaction. This contrasts with the CuZnO(P) catalyst, for which both the C=O hydrogenation and the subsequent C–O hydrogenolysis occurred, leading to the conversion of BHMF to 5-MFA and DMF.

**Recycling of CuZnO catalysts.** Taking into account the influence of the reduction pretreatment on the CuZnO(I) catalyst performance and the reductive nature of the reaction medium, it was worth investigating the cycling behavior of the studied CuZnO catalysts (Table 3). First, the direct reuse of the CuZnO(I) catalyst led to a drastic drop of the activity, with almost no HMF conversion (6%) being observed for the second test. However, when the catalyst was additionally calcined at 300 °C after the first test, a high HMF conversion was maintained at 95%, while a change in the product distribution was observed, with a decrease in the BHMF yield from 91% to 31% together with an increase in the DMF yield from 0% to 34%. This catalyst change with the increase in

the final product of the HMF hydrodeoxygenation reaction may indicate that activation of the catalyst occurred. This activity trend was amplified when performing further consecutive cycling with an intermediate oxidation step while maintaining the HMF conversion within the 96–100% range. At the 3rd cycle, a further change in the product distribution was noted, with a complete disappearance of the BHMF product and a strong increase in the DMF yield till a stable level around 80% ± 5% was obtained for several test cycles.

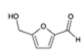
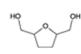
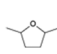
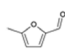
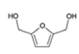
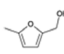
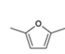
In order to investigate the processes occurring during the cycling procedure, the CuZnO(I) catalyst was firstly reduced under hydrogen at 300 °C to activate the CuZnO catalysts and subsequently oxidized under similar conditions to those used in the cycling tests. The results obtained on the CuZnO(I)-(red)(ox) catalyst showed that only a slight activation occurred, which indicates that other factors plays a key role in the activation of CuZnO(I) catalysts during the cycling tests.

When it comes to the CuZnO(P) catalyst, it displayed a very high activity with full HMF conversion and DMF as the main hydrodeoxygenation product with a DMF yield of 79%. Similarly as in the case of the CuZnO(I) catalyst, direct reuse of the CuZnO(P) catalyst resulted in a decrease in the activity, but in a less pronounced way, maintaining the HMF conversion of 90%, while the DMF yield decreased to 43% and the BHMF yield increased to 26%. Performing an intermediate calcination at 300 °C after the test allowed a total HMF conversion to be achieved for several cycles, with high DMF yields of 92% and 94%. This activity dropped only with the 4th reuse giving BHMF and DMF as the main reaction products with yields of 47% and 41%, respectively.

### Characterization of fresh CuZnO catalysts

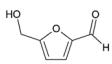
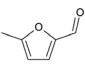
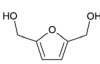
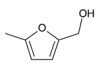
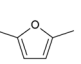
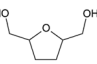
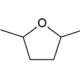
The XRD patterns of the bare ZnO support and of the CuZnO catalysts prepared through the photon-assisted method and the wet impregnation method with different reduction pretreatments are shown in Fig. 1, and the mean crystallite sizes of both the copper-containing phases and the ZnO support are shown in Table 4. They show the diffraction peaks characteristic of ZnO crystallized in the hexagonal wurtzite structure and corresponding to the diffraction of the (100), (002), (101), (102), (110), and (103) planes for the most intense peaks (*P63mc* space group, JCPDS 00-036-1451).<sup>30</sup> In

**Table 2** Influence of the reaction time and catalyst preparation method on the activity of CuZnO catalysts in HMF hydrodeoxygenation

Catalyst	Time [h]	HMF conv. [%] 	Product yield [%]					BHMTFH 	DMTHF 
			5-MF 	BHMF 	5-MFA 	DMF 			
CuZnO(P)	1	93	1	5	31	48	2	3	
	5	100	0	5	6	79	1	9	
CuZnO(I)	0.5	98	4	93	1	0	0	0	
	1	99	5	91	3	0	0	0	
	5	99	2	93	2	0	0	0	

Reaction conditions: 220 °C; 0.3 g of catalyst; 1 g of HMF; 30 ml of dioxane; 30 bar of hydrogen.

**Table 3** Activity and test-cycling behavior in HMF hydrodeoxygenation of CuZnO catalysts

Catalyst	HMF conv. [%] 	Product yield [%]					
		5-MF 	BHMF 	5-MFA 	DMF 	BHMTFH 	DMTFH 
CuZnO(I)	99	2	91	2	0	0	0
CuZnO(I)-r2	6	3	0	3	0	0	0
CuZnO(I)-r2(ox)	95	7	31	7	34	8	1
CuZnO(I)-r3(ox)	100	0	0	0	85	0	15
CuZnO(I)-r4(ox)	96	3	11	5	72	0	4
CuZnO(I)-r5(ox)	99	2	9	4	77	2	6
CuZnO(I)-(red)(ox) <sup>a</sup>	99	5	81	10	2	1	0
CuZnO(P)	100	0	5	6	79	1	9
CuZnO(P)-r2	90	7	26	10	43	1	4
CuZnO(P)-r2(ox)	100	0	0	1	94	0	5
CuZnO(P)-r3(ox)	100	1	0	3	92	0	4
CuZnO(P)-r4(ox)	100	2	47	9	41	1	0
CuZnO(P)-r5(ox)	93	5	47	12	42	0	1

Reaction conditions: 220 °C; 5 h; 0.3 g of catalyst; 1 g of HMF; 30 ml of dioxane; 30 bar of hydrogen. Nomenclature: e.g. the CuZnO(I)-r2 and CuZnO(I)-r2(ox) catalysts correspond to the 2nd test of the CuZnO(I) catalyst without and with an intermediate oxidation treatment at 300 °C, respectively. <sup>a</sup> CuZnO(I)-(red)(ox) catalyst corresponds to the 1st test of the CuZnO(I) catalyst after a reduction treatment under hydrogen at 300 °C followed by an oxidation treatment at 300 °C.

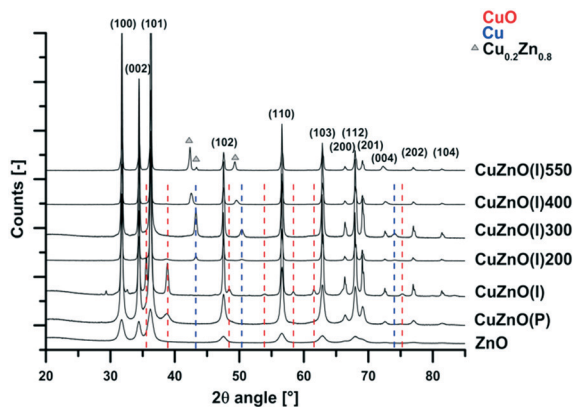
addition to the reflexes from the ZnO support, the XRD patterns of both the CuZnO(P) and CuZnO(I) catalysts exhibited diffraction peaks attributed to the (002), (111), (-202), (020), (202), (-113), (-222) and (222) planes of monoclinic Cu<sup>(II)</sup>O nanoparticles (JCPDS card 01-089-5895). While the as-synthesized ZnO support had a mean crystallite size of 10 nm, the implementation of both preparation methods led to an increase in the mean crystallite size of the ZnO support to 20 nm for the CuZnO(P) catalyst, and to a larger extent to 42 nm for the CuZnO(I) counterpart. As a result, the CuZnO(I) and CuZnO(P) catalysts had a specific surface area of 25 m<sup>2</sup> g<sup>-1</sup> and 33 m<sup>2</sup> g<sup>-1</sup>, respectively, while the bare support exhibited a surface area of 68 m<sup>2</sup> g<sup>-1</sup>.

For both freshly prepared catalysts, a mean CuO crystallite size of 10 nm was observed for CuZnO(P), whereas a

significantly larger mean size of 23 nm was obtained for CuZnO(I) as a result of the final calcination step of the catalyst at 300 °C with exothermic decomposition of the precursor salt. Independently of the preparation method, the CuZnO catalyst can be considered as a CuO–ZnO composite catalyst, since the CuO crystallites do not exhibit significantly smaller mean sizes than the ZnO crystallites, rather than as a ZnO-supported Cu catalyst that would usually consist of smaller sized Cu-based nanoparticles dispersed on the ZnO support.

The nature of the Cu phase progressively turned into metallic Cu with the increase in the reduction temperature, so that both Cu<sup>(II)</sup>O and Cu<sup>0</sup> phases were observed for the catalyst treated at 200 °C, with a mean crystallite size of 13 and 22 nm, respectively, while only reflexes corresponding to the diffraction of the (111), (200) and (220) planes of Cu<sup>0</sup> (JCPDS 01-085-1326) were observed for the CuZnO(I)300 catalyst with no size change.

A further increase in the reduction temperature resulted in the formation of an intermetallic CuZn compound, with the presence of additional reflexes in 2θ at 42.4°, 43.5° and 49.2° at 550 °C attributed to the Cu<sub>0.2</sub>Zn<sub>0.8</sub> alloy phase,<sup>31</sup> with a mean crystallite size of 32 nm. At the intermediate temperature of 400 °C, the observed reflexes might be attributed to an intermetallic CuZn phase with a different composition. By contrast, the mean ZnO crystallite size was not affected by the reduction step under hydrogen and remained within the 42–46 nm range.



**Fig. 1** X-ray diffraction patterns of the ZnO support, the CuZnO(P) catalyst and the CuZnO(I) catalyst with different reduction pretreatments. The crystallographic planes indicated correspond to the diffraction planes of the ZnO support.

### Characterization of used and post-reaction treated catalysts

Fig. 2 and Table 5 show the influence of the 1st catalyst cycling on the XRD patterns of both CuZnO catalysts and on the derived mean crystallite sizes. Besides the reflexes of the

**Table 4** Main properties of the CuZnO catalysts derived from XRD patterns

Catalyst	Cu phase composition	Cu phase mean crystallite size <sup>a</sup> (nm)	ZnO mean crystallite size <sup>a</sup> (nm)
CuZnO(I)550	Cu <sub>0.2</sub> Zn <sub>0.8</sub>	32	44
CuZnO(I)400	Probably inter metallic Cu <sub>x</sub> Zn <sub>y</sub>	20	43
CuZnO(I)300	Cu	24	46
CuZnO(I)200	Cu	22	45
	CuO	13	
CuZnO(I)	CuO	23	42
CuZnO(P)	CuO	10	20
ZnO	—	—	10

<sup>a</sup> Defined as the mean size of the coherently diffracting domains, derived from the Scherrer equation using the classical assumption of spherical crystallites. The full-width at half maximum of the diffraction peaks of ZnO (100), Cu (111), CuO (111) and Cu<sub>0.2</sub>Zn<sub>0.8</sub> (101) planes was used for the estimation.

ZnO support, the pattern of the used CuZnO(I) evidenced the reflexes of the metallic Cu phase, with a mean crystallite size of 28 nm, characterizing the bulk reduction of CuO into metallic Cu during the catalytic reaction under hydrogen pressure. Further recalcination of the used CuZnO(I) resulted in the reoxidation of the metallic copper into both the CuO and the Cu<sub>2</sub>O phase, with a smaller mean crystallite size of 11 nm and 12 nm, respectively. When it comes to the CuZnO(P) catalyst, the reaction induced a reduction of the pristine monoclinic CuO crystallites into cubic Cu<sub>2</sub>O crystallites (JCPDS card 00-005-0667) with a mean crystallite size of 41 nm, whereas a broad peak corresponding to metallic Cu was observed. After the calcination treatment of the used CuZnO(P) catalyst, both the Cu<sub>2</sub>O and the CuO crystallites were observed, with a mean crystallite size of 15 nm and 12 nm. The mean crystallite size of the ZnO support was not affected by the treatments applied, considering the accuracy of the measurements.

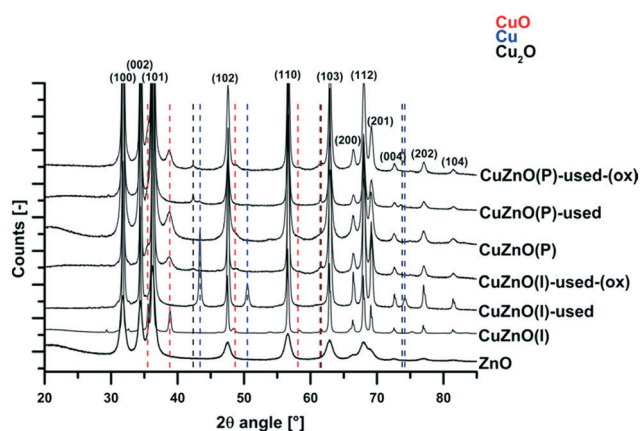
In addition, Rietveld refinement of the diffractograms showed that no incorporation of copper ions within the zinc oxide support lattice occurred, either during the catalyst preparation step or during the reaction at 220 °C under 30

bar of hydrogen or the intermediate reoxidation step after the test regardless of the synthesis method used (Table S1†).

The CuZnO(I) catalyst shows higher temperature stability and the particle size stays nearly stable during the reaction. The reoxidation step allows reaching a smaller particle size that is then kept during the further oxidation cycles (Table S2†). By contrast, the CuZnO(P) catalyst is more prone to changes as the initial photoassisted synthesis treatment was performed at room temperature. Under reductive reaction conditions, larger Cu<sub>2</sub>O nanoparticles are formed, which redispersed to the initial size during their reoxidation step, forming back CuO.

Fig. 3 and 4 show SEM and TEM images, respectively, of selected CuZnO(I) and CuZnO(P) catalysts during the test cycling procedure. The SEM images indicate that the overall morphology of the ZnO-based materials was not modified by the Cu nanoparticle synthesis processes compared to the bare support (Fig. S1†), except for a more marked increase in the mean ZnO particle size in the case of the CuZnO(I) samples compared to the CuZnO(P) counterpart. The electronic structure similarity between Cu and Zn did not enable discrimination between both oxide particles and mainly surface topographic contrast was observed. However, overall EDS analysis evidenced the presence of copper within the catalysts. Only imaging in the back-scattered mode enabled visualization of the distribution of the metallic Cu nanoparticles in the catalysts after the test, as shown in the case of the used CuZnO(P).

Fig. 4a and b show the general morphology of the ZnO support material prepared through the carbonate precipitation method, with interplanar spacings of 0.28 nm and 0.25 nm consistent with the (100) and (101) planes of hexagonal wurtzite ZnO crystallites,<sup>32</sup> and with crystallite sizes in agreement with those derived from the XRD patterns. When it comes to the CuZnO catalysts, whatever the applied treatments, the similarities of the interplanar spacings corresponding to the main planes of ZnO and of both CuO and Cu<sub>2</sub>O crystallites did not allow the specific identification and location of the phases in the different CuZnO catalysts that consisted of oxide crystallites in very close contact. However, overall EDS analysis and mapping STEM images confirmed the presence of copper in both samples (Fig. S2†).



**Fig. 2** X-ray diffraction patterns of the bare ZnO support and both CuZnO(P) and CuZnO(I) catalysts, fresh, after test and after test followed by intermediate calcination at 300 °C. The crystallographic planes indicated correspond to the diffraction planes of the ZnO support



**Table 5** Main physicochemical properties derived from XRD patterns of both CuZnO(I) and CuZnO(P) catalysts, fresh, after test and after test followed by intermediate calcination at 300 °C

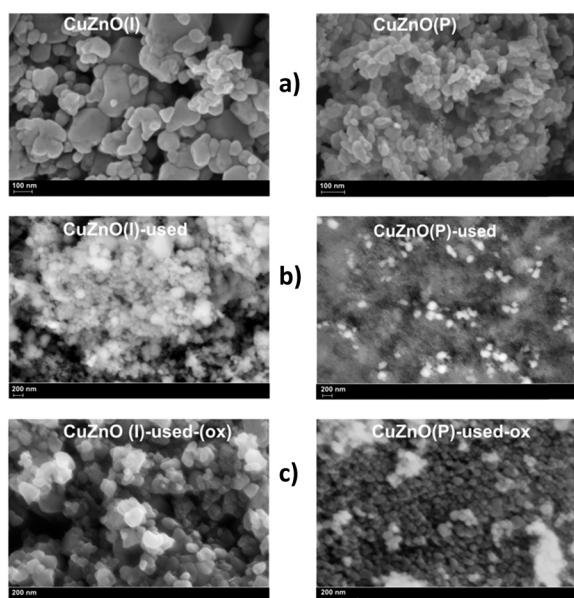
Catalyst	Cu phase composition	Cu phase mean crystallite size <sup>a</sup> (nm)	ZnO mean crystallite size <sup>a</sup> (nm)
CuZnO(I)	CuO	23	42
CuZnO(I)-used	Cu	28	36
CuZnO(I)-used-(ox)	CuO	11	39
	Cu <sub>2</sub> O	12	
CuZnO(P)	CuO	10	20
CuZnO(P)-used	Cu	n.d.	23
	Cu <sub>2</sub> O	41	
CuZnO(P)-used-(ox)	CuO	12	20
	Cu <sub>2</sub> O	15	

<sup>a</sup> Defined as the mean size of the coherently diffracting domains, derived from the Scherrer equation using the classical assumption of spherical crystallites. The full-width at half maximum of the diffraction peaks of ZnO (100), Cu (111), Cu<sub>2</sub>O (200) and CuO (111) was used for the estimation.

The TEM images of both fresh catalysts confirmed as well that the growth of ZnO crystallites was more pronounced during the preparation by the impregnation method than during the photoassisted one.

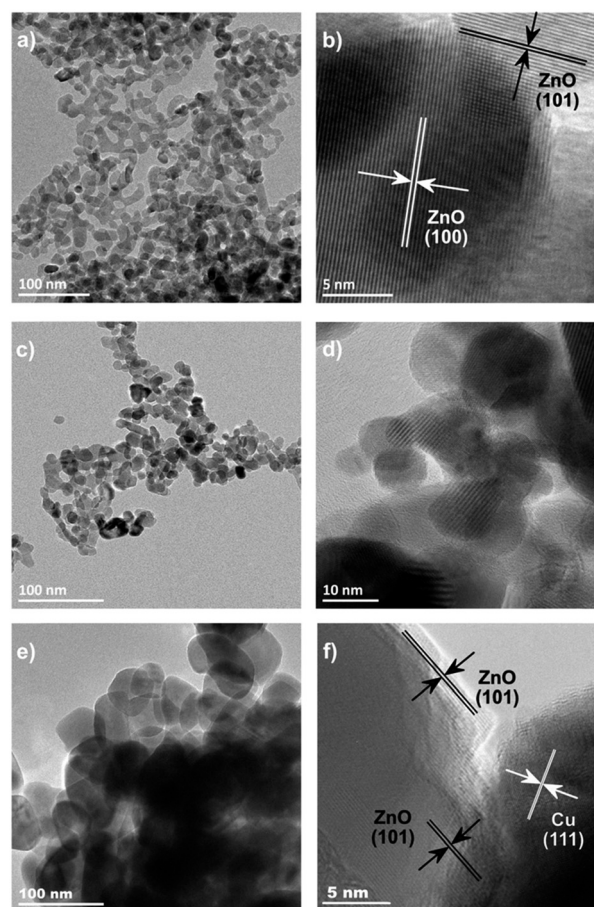
By contrast, the images recorded on the used catalysts reveal the presence of metallic Cu nanoparticles in very close contact with the ZnO crystallites, as evidenced in Fig. 4f, for instance in the case of the catalyst prepared *via* the impregnation method, with the interplanar spacing of 0.21 nm consistent with the (111) planes of metallic copper (JCPDS no. 01-085-1326).

When it comes to the used catalysts after the reoxidation step, the difficulty in visualizing the Cu-based phase within the CuZnO samples confirmed the bulk reoxidation of the metallic Cu nanoparticles observed by XRD (not shown).



**Fig. 3** SEM images of both CuZnO(I) and CuZnO(P) catalysts as a function of the test cycle: (a) fresh, (b) used and (c) used/reoxidized. The right (b) image was taken in the back-scattered mode for evidencing in a more pronounced way the contrast between metallic Cu and ZnO.

The influence of the catalyst preparation method and of the treatment applied (fresh, used and used catalyst after reoxidation step) on the surface state of the CuZnO catalysts



**Fig. 4** TEM images of (a and b) the ZnO support, (c and d) the fresh CuZnO(P) catalyst, (e) the fresh CuZnO(I) catalyst, and (f) the used CuZnO(I) catalyst. The (101) and (100) planes of ZnO have interplanar distances of 0.25 nm and 0.28 nm (JCPDS no.00-036-1451), while the (111) and (002) planes of the CuO phase have 0.23 nm and 0.25 nm interplanar distances (JCPDS no. 01-089-5895), and the (111) planes of the Cu<sub>2</sub>O phase have 0.25 nm interplanar distances, respectively (JCPDS no. 00-005-0667).<sup>33,34</sup>



is shown in Fig. 5 and S3.† The Zn 2p orbital XPS spectra exhibit a single contribution, with the doublet related to Zn 2p<sub>3/2</sub> and 2p<sub>1/2</sub> spin-orbit components of Zn<sup>2+</sup> (Zn–O) surface species, at 1021.1 and 1044.2 eV, in agreement with the literature.<sup>35</sup> While the same surface species were observed on the CuZnO(I) catalyst, it was worth noting the presence of an additional doublet contribution at 1022.8 and 1045.9 eV for the CuZnO(P) catalyst. This higher energy contribution was attributed to Zn<sup>2+</sup> in a different chemical environment and was assigned to Zn–O–Cu bonds. Indeed, in an electrostatic model, the higher electronegativity of Cu compared to Zn resulted in a O → Cu electron transfer in a Zn–O–Cu configuration that would consequently lead to shifting the electronic density of the Zn–O bond towards the oxygen atoms, therefore increasing the electron deficiency of the Zn atoms. This partial substitution of Zn<sup>2+</sup> by Cu<sup>2+</sup> might occur only at the surface of the CuZnO catalyst prepared through the photoassisted synthesis, since ZnO is prone to surface photocorrosion under irradiation.<sup>32,36,37</sup>

In the case of the CuZnO(I) catalyst, no difference was observed in terms of Zn surface species either directly after the reaction on the used catalyst or after the reoxidation of the used catalyst. By contrast, the spectra recorded on the used CuZnO(P) catalyst revealed the appearance of a new doublet contribution at 1019.8 and 1042.9 eV. This lower energy contribution was attributed to Zn<sup>δ+</sup> species (ZnO<sub>x</sub>) that may be formed at the interface with copper under the highly reductive reaction conditions. The presence of partially oxidized Zn<sup>δ+</sup> species was observed by Behrens *et al.* at the defective Cu surface of a high-performance Cu/ZnO/Al<sub>2</sub>O<sub>3</sub> catalyst for methanol synthesis as a result of a dynamic SMSI effect with reduction of ZnO particles leading to partial coverage of the metal particles with ZnO<sub>x</sub>.<sup>38</sup> This additional partially oxidized contribution was removed during the subsequent reoxidation step of the used CuZnO(P) catalyst.

Whatever the preparation method, the Cu 2p orbital XPS spectra show the presence of Cu<sup>2+</sup> species at the surface of the fresh catalysts, with a broad doublet contribution (main

orbital peak at 932.5 eV) and the usual broad and badly resolved satellite features of Cu<sup>2+</sup> species (Fig. S3†). The thinner doublet contribution observed on the used catalysts was in agreement with the formation of metallic copper observed by XRD analysis, although XPS does not allow discriminating between metallic copper and Cu<sup>+</sup> species. Further, the peak asymmetry indicated that surface oxidation of the copper species occurred. The surface of the used reduced catalysts turned back to Cu<sup>2+</sup> during the reoxidation step of both used catalysts, with the observation of broader and slightly shifted peaks.

### The reducibility of the catalysts

The reducibility of the CuZnO catalysts (fresh and after reoxidation treatment) was investigated by TPR measurements. The TPR profile of the fresh CuZnO(I) catalyst presented in Fig. 6a shows a broad reduction peak with several contributions within the 180–400 °C temperature region and a very small effect at 400–650 °C. This complex TPR profile results first from the two-step reduction of the Cu<sup>II</sup> species in CuO to Cu<sup>I</sup> and subsequently to Cu<sup>0</sup> (ref. 39) and from the presence of different types of species differing in terms of size, dispersion, and interaction with the support. The low-temperature small peak (180–220 °C) probably results from amorphous, small-sized, Cu species weakly interacting with the support.<sup>40,41</sup>

The main effect (180–400 °C) is related with the step-wise reduction of CuO that is also directly affected by the presence of crystalline CuO<sub>x</sub> nanoparticles of different sizes, additionally interacting with the support differently – the stronger the interaction, the higher the reduction temperature.<sup>39,42,43</sup>

The final reduction effect at high temperatures in the range of 400–700 °C can be connected with the reduction of Cu<sup>2+</sup> species which are in strong interaction with the support, with further CuZn alloy formation.<sup>44</sup>

After recalcination of the used catalyst, the TPR profile is shifted to lower temperature in comparison to the fresh CuZnO(I), and only one reduction peak is visible, with a maximum at 230 °C. It may be related to a redistribution of smaller CuO crystallites.<sup>45</sup> It shows clearly that the Cu species are more susceptible to reduction.

The TPR profiles of the CuZnO(P) catalysts prepared through the photon-assisted method are presented in Fig. 6b.

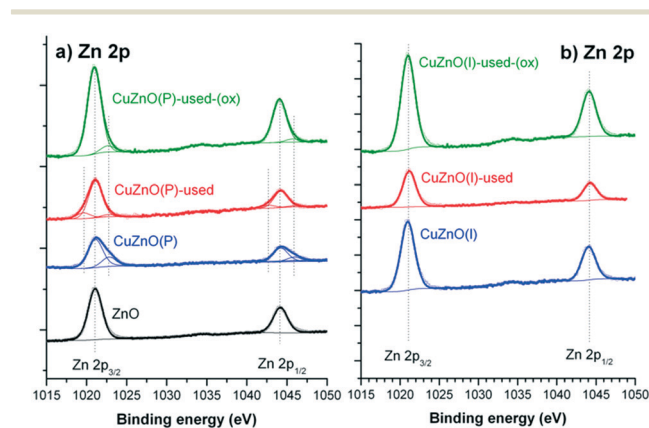


Fig. 5 Influence of the CuZnO catalyst preparation method and of the treatment applied (fresh, used and used catalyst after reoxidation step) on the Zn 2p<sub>3/2</sub> and 2p<sub>1/2</sub> orbital region. (a) Photoassisted method; (b) impregnation method.

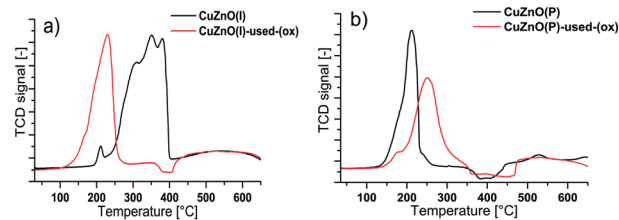


Fig. 6 TPR profiles of (a) the CuZnO(I) and (b) the CuZnO(P) catalysts, fresh and after reoxidation treatment.

The TPR profile of the fresh CuZnO(P) shows two reduction effects, in the 125–290 °C and 400–760 °C temperature range. The first asymmetric peak with a maximum at 210 °C strongly shifted to low temperature when compared to the fresh CuZnO(I) catalyst and may be assigned to the two-step reduction of CuO, but in this case with a much smaller and more uniform crystallite size. The second effect at high temperature, as in the case of the CuZnO(I) catalysts, may be related with the reduction of Cu<sup>2+</sup> in strong interaction with the support.

After oxidation of the used CuZnO(P) catalyst, a slight change of the position of the reduction peak in comparison to fresh catalyst is visible which can occur due to the thermal reduction treatment. However, the changes of the reduction temperature are not so much pronounced like for the CuZnO(I) counterpart, and the reduction temperature maximum for the catalyst after the reoxidation step remains in the same range as for the CuZnO(I) counterpart after a similar cycling treatment.

#### FTIR analysis of the acetone adsorption on the catalyst surface

The first step of the HMF hydrodeoxygenation reaction requires carbonyl group adsorption. Therefore, acetone was chosen as a probe molecule and its adsorption was monitored by FTIR study (Fig. 7). The main, broad band at 1710 cm<sup>-1</sup> can be assigned to the carbonyl group vibrations of acetone<sup>46</sup> and the small band located in the range of 1680–1670 cm<sup>-1</sup> can be assigned to mesityl oxide carbonyl group vibrations.<sup>47</sup> Acetone adsorption allows investigation of the formation of the acid centres of the catalyst due to the formation of mesityl oxide. Mesityl oxide originates from aldol condensation of two adsorbed acetone molecules *via* a dehydration reaction which occurs on acid centers.<sup>48,49</sup>

The highest acetone adsorption is visible for the CuZnO(I) catalyst; however, after reaction, no characteristic band at 1710 cm<sup>-1</sup> is observed any more. It can be related with the formation of Cu<sup>0</sup>. Additionally, it cannot be fully excluded

that active sites are partially blocked by carbon deposits formed during the test.

After recalcination of CuZnO(I), a much smaller band is observed; additionally, a small, broad band at 1680 cm<sup>-1</sup> appears, which can be assigned to the carbonyl group vibrations of mesityl oxide. Therefore it can be assumed that during the postreaction treatment of the CuZnO(I) catalyst, formation of the acidic centres occurs. In the case of the CuZnO(P) catalyst prepared with the photon-assisted deposition method, acetone adsorption is significantly smaller than in the case of CuZnO(I). This might be related with a stronger CuO–ZnO interaction and therefore the presence of the Cu–O–Zn bonds due to the partial dissolution of Cu<sup>2+</sup> ions in the ZnO lattice, which may influence the acetone adsorption.

What is more, interaction of copper oxide with ZnO increases the electron density of Cu by charge transfer from ZnO with the formation of copper species with lower positive charge Cu<sup>(2-δ)+</sup>. This effect is enhanced for low Cu content catalysts and for the small CuO particle size as in the case of CuZnO(P).<sup>50</sup>

Interestingly, for the CuZnO(P) catalyst, the band of mesityl oxide C=O is present also for the fresh catalyst. This can be related with the presence of Zn–O–Cu sites at the surface of the catalyst, as put forward by the XPS study, which can serve as Lewis acid centers, allowing dehydration of the adsorbed molecule. Although after reaction a decrease of the intensity of the acetone C=O group vibration band is observed, in contrast to CuZnO(I), acetone adsorption still occurs, which may also be related with the presence of Zn–O–Cu sites (although to a lower extent) and/or with the formation during the reaction of partially oxidized Zn<sup>δ+</sup> centers or of Cu<sub>2</sub>O species. Further calcination of the used catalyst causes an increase in the amount of adsorbed acetone. What is more, increase of formation of mesityl oxide was also noted, which suggests that further formation of the acid sites occurred.

#### Catalyst stability characterization

In order to investigate the stability of the catalysts FAAS measurements of the reaction liquid and ToF-SIMS measurements of the catalyst surface were performed. FAAS measurements revealed that in the case of the catalyst prepared *via* the wet impregnation method no leaching of the Cu<sup>2+</sup> or Zn<sup>2+</sup> occurs, whereas in the case of the catalyst prepared *via* the photon-assisted deposition method only slight leaching of both copper and zinc ions takes place, with ions released less than 0.3% wt of the initial amount in the catalyst. Therefore, leaching cannot be considered as a reason for catalyst deactivation during recycling tests. ToF-SIMS analysis of the catalyst surface was performed to further investigate the deactivation phenomena of the catalysts (Table 6).

In the case of the CuZnO(I) catalysts, both C<sup>+</sup>/Cu<sup>+</sup> and C<sup>+</sup>/Zn<sup>+</sup> ratios are gradually increasing from around 0.1 for the

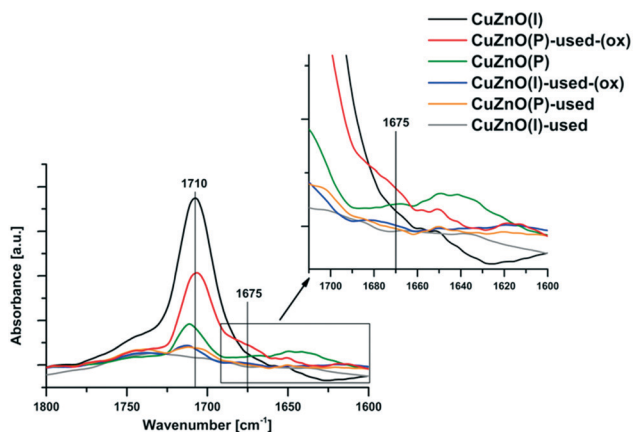


Fig. 7 Acetone-adsorbed FTIR profiles for CuZnO(I) and CuZnO(P) catalysts according to the recycling treatment.

fresh catalyst (that corresponds to the usual background ratio) up to 0.5 for  $C^+/Cu^+$  and 1.5 for  $C^+/Zn^+$  for the catalyst after the 3rd test cycle. Similar observations can be made for the CuZnO(P) catalyst, where both  $C^+/Cu^+$  and  $C^+/Zn^+$  ratios are increasing from 0.086 and 0.161 values up to 1.430 and 3.120, respectively. Therefore, the results indicated that carbon deposition may be a reason for the catalyst deactivation which occurs during the recycling tests.

## Discussion

We believe that the presence of  $Cu^{n+}$  is necessary in the initial reaction step for facilitating the pre-adsorption of HMF on the surface *via* the C=O bond, since it has been reported that both  $Cu^{2+}$  and  $Cu^+$  centers have a pivotal role as far as the C=O bond is concerned.<sup>51</sup> The  $Cu^{n+}$  sites at the catalyst surface can act as electrophilic or Lewis acidic centers for polarizing the C=O bond *via* the lone electron pair in oxygen, with an enhancement of the C=O adsorption and of the activity as a consequence.<sup>52</sup>

This enhancement was noticed in several processes which require a C=O bond hydrogenation, such as the hydrogenation of dimethylxalate to ethanol<sup>53</sup> or the hydrogenation of adipic acid to 1,6-hexanediol.<sup>54</sup> Although a direct relationship between the number of  $Cu^+$  or  $Cu^{2+}$  centers and the activity is only scarcely observed,<sup>54</sup> the role of  $Cu^{n+}$  ions is often related to the stabilization of the reaction intermediates, like the methoxy and acyl species in methyl acetate hydrogenation<sup>53</sup> or in LA hydrogenation.<sup>55</sup>

In our case, the surface of CuZnO(I) exposing  $Cu^{2+}$  sites was characterized by a high adsorption, whereas the high HMF conversion is reached already after 0.5 h of reaction. The same catalyst is fully reduced after the reaction cycle and thus did not exhibit any adsorption, and consequently no HMF conversion in the reaction is obtained when the catalyst is reused as is with no intermediate treatment. This is in contrast to the CuZnO(P) catalyst, which is not fully reduced after reaction – in the presence of the  $Cu_2O$  phase in addition to the metallic copper – and therefore allows HMF adsorption *via* the C=O bond to occur. As a result, HMF conversion can further proceed on the used catalyst during the next test cycle without any intermediate treatment.

**Table 6** The intensity ratios of selected ions calculated on the basis of the ToF-SIMS mass spectra collected from the surface of CuZnO(P) and CuZnO(I) catalysts after tests

Catalysts <sup>a</sup>	$C^+/Cu^+$	$C^+/Zn^+$
CuZnO(I) (fresh)	0.103	0.094
CuZnO(I) after 1st test	0.062	0.119
CuZnO(I) after 3rd test	0.504	1.540
CuZnO(P) (fresh)	0.086	0.161
CuZnO(P) after 1st test	0.245	0.820
CuZnO(P) after 3rd test	1.430	3.120

<sup>a</sup> The catalysts were submitted to an intermediate oxidation step at 300 °C between each test during the cycling procedure.

Although the  $Cu^{n+}$  sites are required for the first step, namely the HMF adsorption on the catalysts *via* the C=O bond, they are however not the active sites for the hydrogenation process. Indeed  $Cu^0$  is formed *in situ* in the process, and its role is related to the dissociation of  $H_2$  and to the reduction of the C=O bond, so that a cooperative effect associated to the presence of metallic and  $Cu^{n+}$  sites is necessary. This is in agreement with literature reports concerning other hydrogenation processes.<sup>56</sup>

The HMF adsorption *via* the C=O bond and the subsequent efficient reduction of the C=O bond enable getting a high yield of BHMF, while the further reduction towards DMF implies C–O hydrogenolysis to take place, for which the presence of both  $Cu^0$  and acid sites is required.

Oxygen vacancies in ZnO that act as Lewis acid sites can be formed at the ZnO–CuO interfacial sites due to the existence of stronger interactions between ZnO and Cu species.<sup>57</sup> The increased synergy within  $ZnO_x$ – $CuO_x$  phases was already proposed as an important factor promoting the activity, particularly in the case of methanol synthesis. Valant *et al.* showed recently that the activity of the Cu–ZnO catalyst in the methanol synthesis is directly correlated to the number of contact points between Cu species and ZnO nanoparticles.<sup>58</sup> On the other hand, Behrens *et al.* proposed that the Cu–ZnO synergy was related to the presence of  $Zn^{\delta+}$  at the Cu surface (steps/defects), which might result from a strong Cu–ZnO interaction allowing a partial coverage of the Cu surface with  $ZnO_x$  under reducing conditions. This could result in the increase in the binding strength of intermediates and in the decrease of reaction barriers in CO hydrogenation.<sup>38</sup>

This may explain why the reaction goes forward towards further hydrogenation products like DMF in the case of the CuZnO(P) catalyst, whereas by contrast the reaction is stopped on the CuZnO(I) catalyst despite the latter showing a slightly higher activity. Lewis acid sites were formed on CuZnO(P) during the photoassisted synthesis procedure as ZnO is prone to surface photocorrosion under irradiation. Their presence was confirmed by the formation of mesityl oxide during the IR study with acetone as the probe molecule. Their formation was noticed also for the used CuZnO(I) catalyst after reoxidation treatment and this directly resulted in pushing the selectivity of the reaction. Additionally, the most active catalyst, CuZnO(P), that allows reaching a high DMF yield had small-sized Cu particles (~10 nm), which probably facilitates the phase contact within the  $CuO_x$ –ZnO material.

Finally, we showed that the catalysts can be further activated during the reaction, and thanks to that the reaction selectivity can be tuned. The possibility of tuning the reaction selectivity was shown already in this reaction, however, only by changing the reaction conditions, such as elevating the temperature or the pressure. Indeed, mild reaction conditions allowed the formation of BHMF, whereas DMF was the main product under harsh conditions.<sup>19</sup> This was however followed by a fast deactivation of the catalyst already in the second reaction cycle.



In our case, the high activity obtained was proposed to result from the formation of Lewis acid sites (Cu–ZnO interfacial sites) as well as from the migration and the redispersion of Cu particles that can occur during both the reduction and the reoxidation treatments.<sup>59,60</sup>

## Conclusions

In this work, we showed that robust 10% CuZnO catalysts allow both BHMf or DMF products to be obtained with high yields from HMF. The selectivity was proposed to depend on the presence of acid sites at the catalyst surface, which might probably correspond to ZnO<sub>x</sub>–CuO and/or Zn–O–Cu interfacial sites. These sites can be formed during the photoassisted synthesis of the CuZnO catalyst or can be created *in situ* in the highly reductive reaction environment. The catalyst prepared at room temperature through the photoassisted method possesses acid sites, which enable direct DMF formation. By contrast, these acid sites were only generated during the reaction on the catalyst prepared *via* the classical wet impregnation method. What is more, we have concluded that high HMF conversion is possible when Cu<sup>2+</sup> and Cu<sup>0</sup> sites are present, as Cu<sup>2+</sup> allows for HMF adsorption *via* the C=O bond, while Cu<sup>0</sup> allows for H<sub>2</sub> dissociation and reduction.

Before subsequent reaction cycles, reoxidation of the CuZnO catalyst needs to be performed, which can lead to the redispersion of Cu particles. This oxidative treatment allows one to obtain active and selective catalysts for several reaction cycles. By contrast, performing the reduction of the CuZnO catalyst at a high temperature (300–550 °C) before the reaction can result in CuZn alloy formation and only marginal HMF conversion can be obtained.

## Conflicts of interest

There are no conflicts to declare.

## Acknowledgements

The authors gratefully acknowledge that this work was financially supported by a grant from the National Center of Science (NCN) in Krakow (Poland) (2016/22/E/ST4/00550). This research was co-funded by the EU Erasmus+ program. T. Dintzer and V. Papaefthimiou (ICPEES) are thanked for performing SEM and XPS analysis, respectively. C. Lefèvre (IPCMS Strasbourg) and W. Maniukiewicz (LUT) are thanked for contributing to XRD.

## Notes and references

- S. Shafiee and E. Topal, *Energy Policy*, 2009, 37, 181.
- R. A. Sheldon, *Green Chem.*, 2014, 16, 950.
- A. M. Ruppert, K. Weinberg and R. Palkovits, *Angew. Chem., Int. Ed.*, 2012, 51, 2564.
- J. J. Bozell and G. R. Petersen, *Green Chem.*, 2010, 12, 539.
- Y. Jiang, A. J. J. Woortman, G. O. R. A. van Ekenstein, D. M. Petrović and K. Loos, *Biomacromolecules*, 2014, 2482.
- L. Hu, J. Xu, S. Zhou, A. He, X. Tang, L. Lin, J. Xu and Y. Zhao, *ACS Catal.*, 2018, 8, 2959.
- R. Daniel, G. Tian and H. Xu i S. Shuai, *Fuel*, 2012, 99, 72.
- G. Tian, R. Daniel, H. Li, H. Xy, S. Shuai and P. Richards, *Energy Fuels*, 2010, 24, 3898.
- S. Chen, R. Wojcieszak, F. Dumeignil, E. Marceau and S. Royer, *Chem. Rev.*, 2018, 118, 11023.
- M. Besson, P. Gallezot and C. Pinel, *Chem. Rev.*, 2014, 114, 1827.
- X. Wang, X. Liang, J. Li i and Q. Li, *Appl. Catal., A*, 2019, 576, 85.
- J. Luo, M. Monai, C. Wang, J. D. Lee, T. Duchon, F. Dvorak, V. Matolin, C. B. Murray, P. Fornasiero and R. J. Gorte, *Catal. Sci. Technol.*, 2017, 17, 1735.
- J. M. Requies, M. Frias, M. Cuezva, A. Iriondo, I. Agirre and N. Viar, *Ind. Eng. Chem. Res.*, 2018, 57, 11535.
- R. R. Velarde, A. Grigotopoulos, N. Perret, M. Zanella, A. P. Katsoulidis, T. D. Manning, J. B. Claridge and M. J. Rosseinsky, *Green Chem.*, 2017, 19, 1701.
- M. A. Lilga, R. T. Hallen, T. A. Werpy, J. F. White, J. E. Holladay, J. R. Frye and A. H. Zacher, *U.S. Pat. Application* 2007/0287845, 2007.
- M. S. Gyngazowa, L. Negahdar, L. C. Blumenthal and R. Palkovits, *Chem. Eng. Sci.*, 2017, 173, 455.
- D. P. Duarte, R. Martinez and L. J. Hoyos, *Ind. Eng. Chem. Res.*, 2016, 55, 54.
- Y. Roman-Leshkov, C. J. Barret, Z. Y. Liu and J. A. Dumesic, *Nature*, 2007, 447, 982.
- Y. Zhu, X. Kong, H. Zheng, G. Ding, Y. Zhu and Y.-W. Li, *Catal. Sci. Technol.*, 2015, 5, 4208.
- Y. Liu, M. M. Mellmer, D. M. Alonso and J. A. Dumesic, *ChemSusChem*, 2015, 8, 3983.
- A. Yepez, A. Pineda, A. Garcia, A. A. Romero and R. Luque, *Phys. Chem. Chem. Phys.*, 2013, 15, 12165.
- Z. Zhang, C. Wang, X. Gou, H. Chen, K. Chen, X. Lu, P. Ouyang and J. Fu, *Appl. Catal., A*, 2019, 570, 245.
- G. Bottari, A. J. Kumalaputri, K. K. Krawczyk, B. L. Feringa, H. J. Heeres and K. Barta, *ChemSusChem*, 2015, 8, 1323.
- L. B. McCusker, R. B. Von Dreele, D. E. Cox, D. Louer and P. Scardi, *J. Appl. Crystallogr.*, 1999, 32, 36.
- J. Rodriguez-Carvajal, *Phys. B*, 1993, 192, 55.
- M. S. S. Doniach, *J. Phys. C: Solid State Phys.*, 1970, 3, 285.
- D. A. Shirley, *Phys. Rev. B: Solid State*, 1972, 5, 4709.
- B. Seemala, C. M. Cai, C. E. Wyman and C. Christopher, *ACS Catal.*, 2017, 76, 4070.
- D. Hu, H. Hu, H. Zhou, G. Li, C. Chen, J. Zhang, Y. Yang, Y. Hu, Y. Zhang and L. Wang, *Catal. Sci. Technol.*, 2018, 8, 6091.
- S. Srivastava, G. C. Jadeja and J. Parikh, *J. Mol. Catal. A: Chem.*, 2017, 426, 244.
- T. B. Massalski and H. W. King, *Acta Metall.*, 1962, 10, 1171.
- M. Brzezinska, P. Garcia-Munoz, A. M. Ruppert and N. Keller, *Materials*, 2018, 11, 2260.
- Y. Liu, L. Zhong, Z. Peng, Y. Song and W. Chen, *J. Mater. Sci.*, 2010, 45, 3791.
- M. H. Kim, B. Lim, E. Lee and Y. Xia, *J. Mater. Chem.*, 2008, 18, 4069.



- 35 M. Wang, L. Jiang, E. Jung, E. J. Kim and S. K. Hahn, *RSC Adv.*, 2015, 5, 87496–87503.
- 36 X. Ma, H. Li, T. Liu, S. Du, W. Qiang, Y. Wang, S. Yin and T. Sato, *Appl. Catal., B*, 2017, 201, 348.
- 37 C. Han, M. Yang, B. Weng and Y. Xu, *Phys. Chem. Chem. Phys.*, 2014, 16, 16891.
- 38 M. Behrens, F. Studt, I. Kasatkin, S. Kuhl, M. Havecker, F. Abild-Pedersen, S. Zander, F. Girsdies, P. Kurr, B.-L. Kniep, M. Tovar, R. W. Fischer, J. K. Norskov and R. Schlögl, *Science*, 2012, 336, 893.
- 39 C. A. Galvan, J. Schumann, M. Behrens, J. L. Fierro, R. Schlögl and E. Frei, *Appl. Catal., B*, 2016, 195, 104.
- 40 J. Agrell, M. Boutonnet, I. Melian-Cabrera and J. L. G. Fierro, *Appl. Catal., A*, 2003, 253, 201.
- 41 G. J. Millar, I. H. Holm, P. J. R. Uwins and J. Drennan, *J. Chem. Soc., Faraday Trans.*, 1998, 94, 593.
- 42 T. Shishido, M. Yamamoto, D. Li, Y. Tian, H. Morioka, M. Honda, T. Sano and K. Takehira, *Appl. Catal., A*, 2006, 303, 62.
- 43 D. Ji, W. Zhu, Z. Wang and G. Wang, *Catal. Commun.*, 2007, 8, 1891.
- 44 R. Yang, X. Yu, Y. Zhang, W. Li and N. Tsubaki, *Fuel*, 2008, 87, 443.
- 45 J. Agrell, H. Birgersson, M. Boutonnet, I. Melian-Cabrera, R. M. Navarro and J. L. G. Fierro, *J. Catal.*, 2003, 219, 389–403.
- 46 D. Syomin and B. E. Koel, *Surf. Sci.*, 2002, 498, 53.
- 47 A. G. Panov and J. J. Fripiat, *J. Catal.*, 1998, 178, 188.
- 48 C. Barakat, P. Gravejat, O. Guaitella, F. Thevenet and A. Rousseau, *Appl. Catal., B*, 2014, 147, 302.
- 49 A. Panov and J. J. Fripiat, *Langmuir*, 1998, 14, 3788.
- 50 Y. Okamoto, K. Fukino, T. Imanaka and S. Teranishi, *J. Phys. Chem.*, 1983, 87, 3747.
- 51 V. A. Rogov, F. Serebryakov, N. M. Dobrynkin and V. V. Popovskii, *React. Kinet. Catal. Lett.*, 1989, 40(2), 195–200.
- 52 J. Szanyi and M. T. Paffett, *Catal. Lett.*, 1997, 43, 37–44.
- 53 E. K. Poels and D. S. Brands, *Appl. Catal., A*, 2000, 83, 191.
- 54 J.-W. Jiang, C.-C. Tu, C.-H. Chen and Y.-C. Lin, *ChemCatChem*, 2018, 10, 5449.
- 55 B. Zhang, Y. Chen, J. Li, E. Pippel, H. Yang, Z. Gao and Y. Qin, *ACS Catal.*, 2015, 5, 5567.
- 56 J. Gong, H. Yue, Y. Zhao, S. Zhao, L. Zhao, J. Lv, S. Wang and X. Ma, *J. Am. Chem. Soc.*, 2012, 134, 13922.
- 57 H. Lei, R. F. Nie, G. Q. Wu and Z. Y. Hou, *Fuel*, 2015, 154, 161–166.
- 58 A. Le Valant, C. Comminges, C. Tisseraud, C. Canaff, L. Pinard and Y. Pouilloux, *J. Catal.*, 2015, 324, 41.
- 59 J.-D. Grunwaldt, A. M. Molenbroek, N.-Y. Topsøe, H. Topsøe and B. S. Clausen, *J. Catal.*, 2000, 194, 452.
- 60 M. S. Spencer, *Top. Catal.*, 1999, 8, 259.